Improvement in time-domain induced polarization data quality with multi-electrode systems by separating current and potential cables

Dahlin, Torleif; Leroux, Virginie

Published in:
Near Surface Geophysics

DOI:
10.3997/1873-0604.2012028

2012

Near Surface Geophysics, 2012, **10**, 545-565 doi:10.3997/1873-0604.2012028

Improvement in time-domain induced polarization data quality with multi-electrode systems by separating current and potential cables

Torleif Dahlin* and Virginie Leroux

Engineering Geology, Lund University, Lund, Sweden

Received May 2011, revision accepted April 2012

ABSTRACT

Measuring induced polarization in the time domain with relatively compact multi-channel multi-electrode systems is attractive because of the simplicity of the procedure and thus its efficiency in the field. However the use of this technique is sometimes discouraged by the bad quality of the measurements in cases of high electrode contact resistances that can render data interpretation infeasible or at least unreliable. It is proposed that capacitive coupling in the multi-core electrode cables has a significant role in creating this problem.

In such cases separation of current and potential circuits by using separate multi-conductor cable spreads can yield significant improvement in data quality. The procedure is relatively simple and can be implemented with common resistivity and time-domain IP equipment.

We show here three field examples from Southern Sweden, all measured as 2D electrical imaging sections. The first one is an example where the use of a single cable spread is sufficient thanks to moderate electrode contact resistance and high signal levels. The following two examples are from sites where induced polarization measurements could not yield consistent results using only a single multi-conductor cable spread. Useful results were subsequently obtained by using separate cable spreads.

The first example is a 280 m long line measured over an old covered municipal waste deposit where the waste body stands out as a zone of high chargeability. The second example is a 120 m line measured on a sandy glaciofluvial structure that is host to an aquifer of regional importance. The improvement led to discrimination between materials of different grain sizes, with potential bearing for understanding the aquifer. The third example is a 300–400 m line measured across an esker lying on clay till. The improvement led to a clear visualization of the esker and to the identification of a possible fault in the underlying gneissic bedrock.

In all cases pseudosections and examples of chargeability decay curves are shown and discussed as tools for assessing data quality. Inversion results are shown together with background geological information and it is concluded that they are in good agreement.

INTRODUCTION

The induced polarization method was first extensively used in mining applications from the 1950s, due to the characteristic response of disseminated ore, undetectable by other geophysical methods, which made its success (see Collett 1990; Seigel *et al*. 2007). Its potential in hydrogeological and environmental applications was recognized early on (e.g., Vacquier 1957) but the method started to be extensively used in this field only in the last 20 years. This is due to instrumental and methodological developments but also probably to the more restricted economical resources in environmental applications compared to mining.

*torleif.dahlin@tg.lth.se

In near-surface applications induced polarization has shown to be especially useful for delineating landfills (e.g., Carlson *et al*. 1999; Iliceto *et al*. 1999; Dahlin *et al*. 2010), mapping pollutant plumes (e.g., Abu-Zeid *et al*. 2004; Sogade *et al*. 2006) and in hydrogeological applications (e.g., Martinho and Almeida 2006), where one hopes to be able to estimate hydraulic conductivity (e.g., Hördt *et al*. 2007).

Induced polarization can be quantified using a number of different parameters, e.g., chargeability in the time domain, frequency effect, phase and amplitude in the frequency domain. Although comparable, these measurements are not strictly equivalent (e.g., Zonge *et al*. 1972). Comparing results obtained at different sites with different measuring equipment can as a

consequence be difficult and remains essentially qualitative. Nevertheless some rough equivalence relations exist and are applicable (see e.g., Bertin and Loeb 1972; Sumner 1976; Slater and Lesmes 2002; Loke 2011). Material discrimination and detailed interpretation remain more straightforward in the frequency domain but the time required by the measurements is a serious limitation to the use of the method. Since it is much faster to measure and since significant frequency information is potentially contained in a single decay, time-domain induced polarization remains attractive for most practical applications.

A few methods exist for interpreting time-domain induced polarization in terms of spectral IP (e.g., Hördt *et al*. 2006), also referred to as frequency-dependent complex resistivity. Some authors (Soininen 1984; Ghorbani *et al*. 2007) have pointed out the difficulty of extracting spectral information from time-domain induced polarization data but standard time-domain IP is already useful in many cases. However, difficulties encountered at some sites with high contact resistances can discourage its use. Rapid and reliable data acquisition procedures in the field, as well as ways to assess data quality and reliability are needed and they are the subject of the present article, with an emphasis on practical ways to reduce capacitive coupling with common multi-electrode equipment.

BACKGROUND

Frequency-domain IP is traditionally measured using separate receiver and transmitter units and separate electrode layouts. Dipole-dipole or pole-dipole arrays are commonly used, where one motivation is that coupling between the transmitter and receiver layouts can be avoided. For the measurement of frequency-domain spectral IP in an extended frequency range the coupling problem has been addressed by digitizing the potentials at the receiver electrodes and transmitting the digital data via an optical fibre in order to avoid metal conductors that can lead to coupling.

Time-domain IP-resistivity multi-electrode equipment commonly used in near-surface investigation classically comprises a transmitter, a receiver and a system for switching between the electrodes to be used. These units can be integrated into a single instrument, or they can be separate. The transmitted currents are much lower than those used in mining applications, typically from a few tens of mA to one or a few A. The length of the lines measured lies between a few tens of metres to hundreds of metres. The input impedance of the receiver is generally high (a few tens of MΩ) and some low-pass filtering is usually applied. The multi-conductor cables used are generally non-shielded. Non-polarizable electrodes are sometimes used but simple steel electrodes can be used as well, since they are comparably stable (LaBrecque and Daily 2008). It has been shown that steel electrodes can yield equivalent results, provided that an instrument with suitable properties is used and a correction for the drift of the background potential is applied (Dahlin *et al*. 2002).

The speed of the measurement is significantly increased by the simultaneous use of several measurement channels and in this respect, among the classical four-electrode arrays, the multiple gradient can be recommended, since it has been shown to have adequate sensitivity and resolution (Dahlin and Zhou 2006). This array can furthermore provide relatively large potentials and a high signal-to-noise ratio in resistivity measurements. Depending on the site and aim of the investigation, the duration of the measuring cycle can possibly be reduced and the measurement can go even faster.

The measured parameter is the integral chargeability over one or a series of successive time windows, also called gates. The last instrument we used even allows the recording of the full transmitted and received signals with a 1 ms sampling interval. *A posteriori* assessment of the noise level and, if needed, recalculation of chargeability then becomes possible.

However, with this kind of equipment significant electromagnetic coupling can be an issue. It can be divided into two main components; inductive coupling and capacitive coupling.

Capacitive coupling

The capacitive coupling is simply defined here as current leaks from high-potential surfaces or conductors to low-potential surfaces or conductors. Capacitive coupling is most severe at early times after a change in the transmitted current and decays with time, or expressed differently, it increases with increasing frequency. Large electrode resistance will make it worse because the output voltage required in order to transmit the desired current increases and at the same time the measured signal may decrease due to less current being transmitted. A theoretical description in the frequency domain was given by Nielsen (2006) where the importance of keeping low contact resistance when performing induced polarization measurements was emphasized. The capacitive coupling will also increase with increasing cable length because the total capacitance increases in proportion to the cable length. At the same time the signal decreases with increasing electrode separations as the geometry factor increases and hence the signal will more easily drown in coupling noise. However it will also decrease rapidly with increasing distance between conductors or surfaces (with the square of the distance, based on a simple estimation of the capacitance for a cylindrical capacitor).

Another way to reduce capacitive coupling is to use shielded cables and some theoretical considerations are given in Wait (1959). As noted by Radic (2004), three main capacitive couplings can be identified: between transmitter and receiver cables, between soil and cables and between two receiver cables. In the experiments presented here, in which we separate the current transmission and potential receiving cables, we only address the reduction of the first one.

One data acquisition system on the market offers a so-called dual mode cable with duplicate take-outs at each electrode point, where the idea is to allow a connection of both a steel electrode for current transmission and a non-polarizable electrode next to it for potential measurement. This system will, however, in itself not reduce the coupling in the cable since the conductors are still running parallel inside the same multi-core cable.

Inductive coupling

The direct capacitive coupling between wires is only one part of the more general electromagnetic coupling, where the other part is the inductive coupling. Electromagnetic coupling is generally dependent on the geometry of the wires and on the ground investigated. A review of its theory was given by e.g., Nielsen and Baumgartner (2006). Larger effects are observed and expected for longer cables. Here one should note that the classical recommendation to use dipole-dipole arrays cannot apply to common multi-electrode systems where the transmitter and receiver are close to each other and where conductors run parallel inside the multi-core cables. Inductive coupling is usually assumed to take place early after current turn-off and is commonly assumed to be negligible after a certain time-delay in time domain measurements. However this assumption might not always be verified. A number of computations and even correction procedures have been suggested for frequency domain measurements (e.g., Hohmann 1973; Wynn and Zonge 1975; Pelton *et al*. 1978; Routh and Oldenburg 2001) but the elimination of inductive coupling is difficult and even disputable (see e.g., Swift and Hohmann 1975; Wait and Gruszka 1986). Authors have consequently recommended that it should be included in the interpretation (see e.g., Nielsen and Baumgartner 1986; Wait 1986), since the same range of frequency is affected by both induced polarization and induction effects and their effects show some similarity (e.g., Major and Silic 1981; Nielsen and Baumgartner 2006).

A conventional inversion method was applied to the time-domain IP data discussed in the present work, hence inductive coupling was not considered. However, although it is here beyond our scope, a more thorough investigation of electromagnetic effects in time-domain IP measurements is recommended to determine in what respect such an approach can be considered as a reasonable approximation.

Background potentials

The potential measured between two electrodes while the current is not transmitted will generally be other than zero due to several factors such as streaming potentials, electro-chemical reactions between the electrode and the ground, telluric currents, power grid leakage, etc. The magnitude of the electro-chemical reactions depends on the type of electrodes, where so-called non-polarizable electrodes give small potentials (often tens of mV or less) whereas stainless steel electrodes give large potentials that can reach hundreds of mV (e.g., LaBreque and Daily 2008). When the current is transmitted through a steel electrode it is charged up (often several hundred mV) and the potential decays exponentially during tens of minutes after the current has been turned off (Dahlin 2001). If such an electrode is used for measuring the potential shortly after transmitting the current via the same electrode, the decay will be superimposed on the potential induced in the current measuring cycle, which may be magnitudes smaller.

METHOD

Instruments

We used different versions of the ABEM Lund Imaging System for measuring resistivity and induced polarization in the time domain. At all sites measurements were taken using a research prototype modification of the standard system, comprising a Terraohm RIP924 receiver, an ABEM Booster SAS2000 current transmitter and one or two ABEM Electrode Selector ES464. The whole system was controlled by a portable computer. The receiver unit has 8 input channels with available input ranges of ±1V and ±10V, based on 24 bit sigma-delta AD-converters. All input channels are galvanically insulated from each other. The input impedance of this instrument is larger than 70 MΩ. The maximum transmitter output is 400V or 500mA for a maximum power of 40W. This data acquisition system does not measure the contact resistances. However, by knowing the limitations in terms of maximum transmitted voltage for the different current levels of the transmitter, it is possible to estimate the range of the contact resistances from actual transmitted currents.

At the Knivsåsen site measurements were repeated with an ABEM Terrameter LS, with the receiver, transmitter, electrode selector and computer integrated. In addition an Electrode Selector ES10-64C was used. This instrument has 12 measuring channels based on 24 bit sigma-delta AD-converters, plus two additional measuring channels for monitoring the transmitter. The input ranges are ±2.5 V, ±15 V and ±1000 V, with input impedances larger than 100 MΩ, 30 MΩ and 20 MΩ respectively. All input channels are galvanically insulated from each other. The maximum transmitter output is 600V or 2500 mA for a maximum power of 250 W. This instrument can also record the transmitted and received signals with a 1 ms sampling interval. With this instrument the electrode contact can be estimated using the 'Focus One' technique, in which the contact resistance of each electrode is measured against all the remaining electrodes. This technique can be expected to give an estimation of the maximum level of the electrode contact. Threshold values for acceptable contact resistance are set by the operator, so that electrodes with poor grounding can be identified and the contact improved before measurements start.

Electrodes and cables

Stainless steel electrodes were used throughout. They were connected to the respective relay switches and instruments via standard non-shielded multi-electrode cables. At all sites measurements were carried out using standard single cable array spreads (Fig. 1a). At sites 2 and 3 measurements were also carried out with double layouts with two complete cable spreads in parallel (Fig. 1b). One cable layout was placed on each side of the line of electrodes and shifted half a take-out spacing so that every second electrode was connected to each cable spread. With this arrangement every second electrode is only used for current transmission and the electrodes in-between are only used for potential measurement. After completing a set of measurements

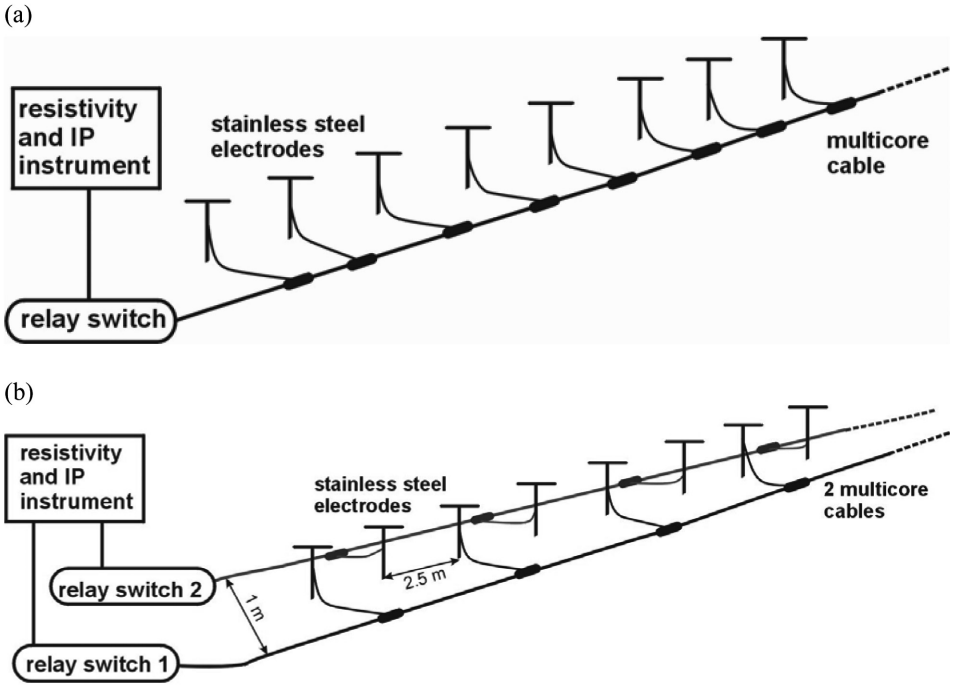

FIGURE 1
Principle sketch showing; a) standard single cable spread and b) separated cable spread for current transmission and potential measurement. For the separated spread setup the electrode separation will be half the electrode take-out spacing in case the cables are stretched. The separations between the cables spreads were around 1 m in all tests but the electrode separation varied. In the tests presented in this paper each spread consisted in up to four cables that were linked together and the instrument and relay switches connected at the midpoint of a full spread.

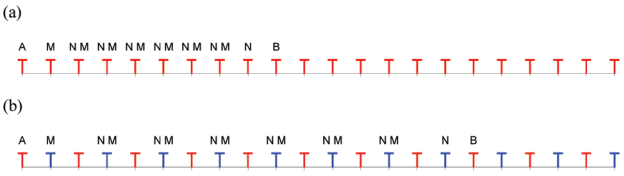

FIGURE 2
Sketch illustrating minimum electrode separation for multiple gradient array measurement (A, B = current electrode, M, N = potential electrode); a) measured with standard single cable spread and b) separated cable spread for current transmission and potential measurement. In the separated cable spread case every 2nd electrode is only used for current transmission and the electrodes in-between are only used for potential measurement, which means that the minimum potential electrode separation is twice the electrode spacing.

the cable connections were switched, so that the current electrodes became potential electrodes and vice versa and an identical but mirrored measurement sequence was carried out. This arrangement means that we were not able to measure in exactly the same standard cable spread, as illustrated in Fig. 2, but the data cover is comparable. A drawback is that the minimum spacing for the potential electrodes was twice the actual minimum electrode spacing, which may affect the resolution.

Measurement setup

Depending on grounding conditions of the test line and the instrument used between 2–200 mA were transmitted. All measurements were carried out using a multiple gradient array according to the sketch in Fig. 2.

The current cycle used is a +/0/-/0 sequence (50% duty cycle), with a 1–1.1 s pulse length. The chargeabilities were measured in 10 time windows with 100 ms fixed duration for the first instrument used and with time windows varying from 20–180 ms for the second one, starting 10 ms after current turn-off. The signals were automatically corrected for variation in the background potentials via measurement of the potential before and after each measurement cycle.

Data analysis, processing and inversion

In order to evaluate data quality the measured data sets were plotted as pseudosections of apparent resistivity and apparent chargeability using linear interpolation that reveals outliers clearly (via the software Erigraph). The IP decay curves were plotted (using the software Aarhus Workbench) as a quality check. Data were inverted to create model sections of the resistivity and chargeability of the ground. The most recent version of Res2dinv (see Loke 2010) at the time was used to invert the sum of the chargeability over the whole measured decay. It uses the method described by Oldenburg and Li (1994). In all cases robust (L1-norm type) inversion was used since there are strong contrasts in resistivity at all the test sites. In addition, we also plotted normalized chargeability following the approach suggested by Slater and Lesmes (2002). In the case of robust inversion the software calculates the mean model residual as the arithmetic mean of the absolute value of the differences between either the logarithm of the measured apparent resistivity and the logarithm of the computed value, or between the measured and computed apparent chargeability.

RESULTS WITH INTERPRETATION

Example 1: Ekeboda

Site description

The Ekeboda landfill has an area of about 20 000 m^2 and is situated in a small valley in the municipality of Hörby in Southern Sweden. The landfill was in use between 1965–1978, with illegal dumping continuing until the mid 1980s. The landfill contains domestic waste, construction, demolition and industrial waste as well as other hazardous waste such as pesticides and mineral oils. The major part of the waste was burned during the early years but later on it was deposited without treatment. The waste has been deposited on natural ground, comprised of sandy till with underlying bedrock of sandstone or possibly gneissic rock (SGU 2000). The covering layer consists of various soils, of which no precise record has been kept. At present, the leachate is collected and transported to the local water treatment facility.

Attempts were made to drill into the waste deposit at several points with a small geotechnical drill rig but it only penetrated up to 1.2 m of rather coarse grained cover material before it reached waste material that could not be penetrated. Outside the waste deposit to the west the groundwater level was found at 5.2 m depth. To the east of the deposit, at the foot of the slope, the groundwater reaches the surface in wet spots and artesian groundwater was found in 4.4 m deep drilling (Johansson and Jones 2007).

Data acquisition

Twelve profiles were measured at the Ekeboda site (Johansson *et al*. 2007) in order to map the extension of the landfill. Only one is presented here but they all present similar characteristics. A single cable spread layout with 2 m electrode spacing was used for this profile, giving a total layout length of 160 m. No particular efforts were needed to provide an acceptable electrode contact at this site. By roll-along a 280 m long profile, consisting in 2177 data points, was measured in less than one day by two inexperienced students. The transmitted current was in the range 20–200 mA and 2 stacks were used for the data points. The elec-

TABLE 1

Transmitted current (I), signal levels in terms of measured average potential difference for the resistance (V_R), example IP time windows ($V_{IP(1)}$ & $V_{IP(10)}$) and background potential levels (V_{backgr}) for the data recorded on the Ekeboda test line with separated current and potential cables.

Parameter	I/[mA]	V_R/[mV]	$V_{IP(1)}$/[mV]	$V_{IP(10)}$/[mV]	V_{backgr}/[mV]
Range	20–200	7.4–5200	0.15–120	0.019–28	0–1500
Median	100	100	5.3	1.0	20

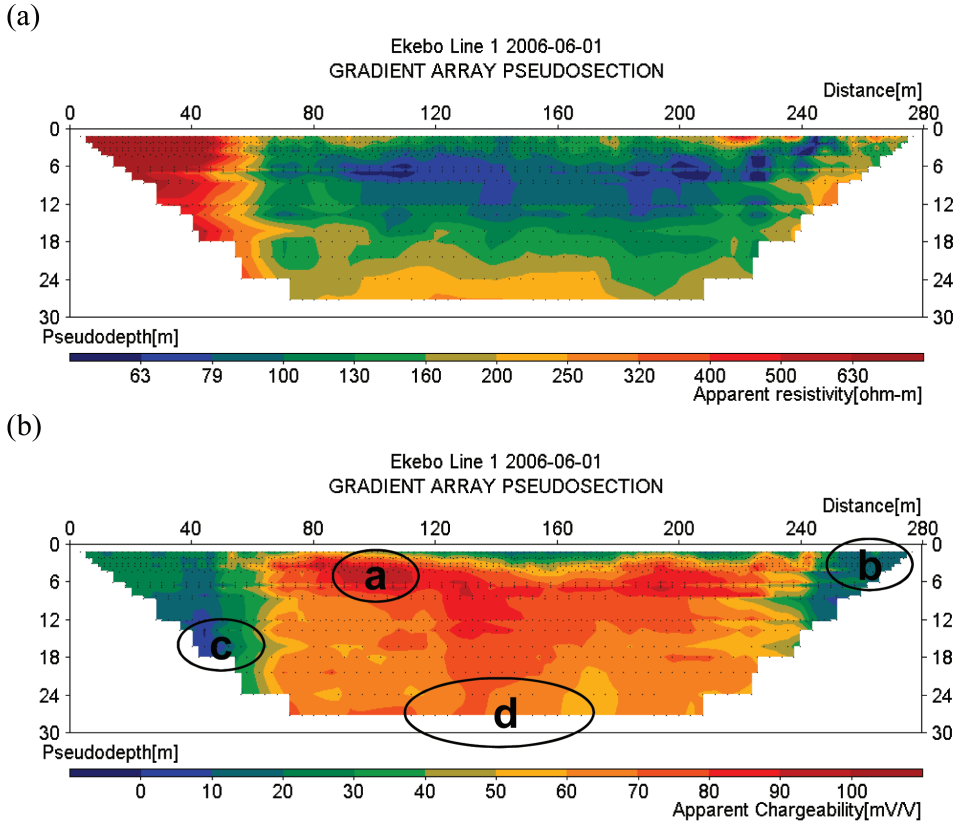

FIGURE 3

Pseudosections from Ekeboda measured with single cable spread for current transmission and potential measurement; a) apparent resistivity and b) apparent chargeability for time window 10–110 ms. IP decay curves from the marked areas are shown in Fig. 4.

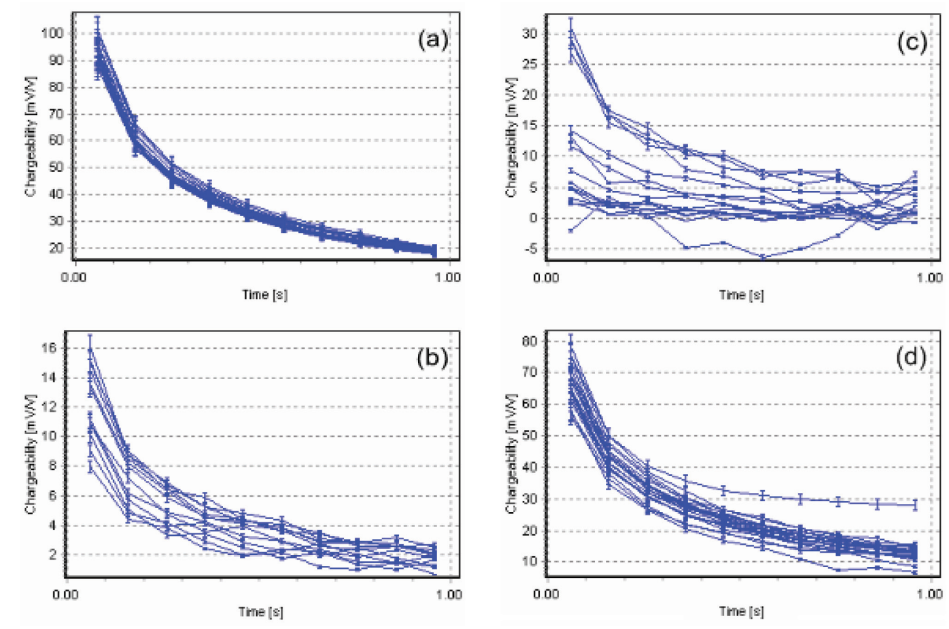

FIGURE 4
IP decay curves from Ekeboda measured with single cable spread for current transmission and potential measurement. The parts of the pseudosection from which each group of decay curves were gathered are marked in Fig. 3. Note that the chargeability scale differs between the diagrams.

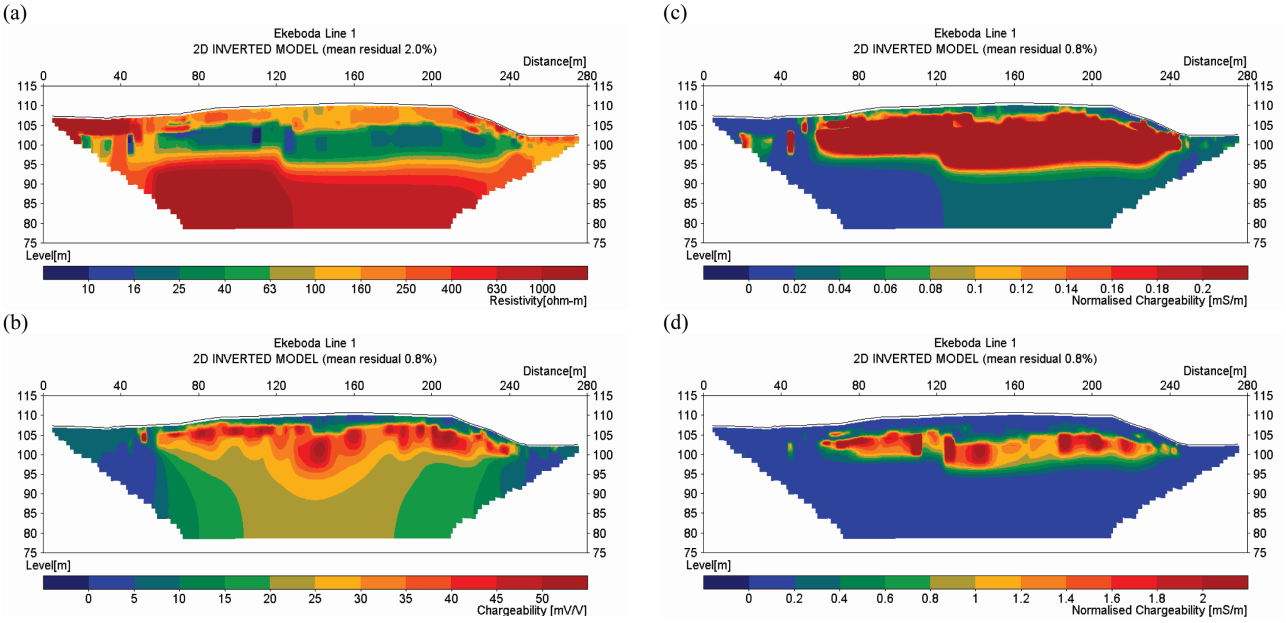

FIGURE 5
Inverted model sections from Ekeboda line 1: a) resistivity, b) chargeability, c) normalized chargeability, d) normalized chargeability with alternative scale.

trode contact resistances were estimated to lie between a few hundred to a few thousand Ω. The signal level was in the range 1–800 mV for the DC resistivity (Table 1), with a median of 8.8 mV. For the IP data the signals were a fraction of that, with median values decaying from 0.47–0.095 mV from time windows 1–10 and the smallest measured signals being a few μV. The maximum background potential level was 1500 mV.

Results

The resistivity and IP data appear to be of high quality for this site, judging by the consistent pseudosections in Fig. 3. The IP data are characterized by high chargeabilities in most of the central part of the profile that was measured over the covered waste deposit. Most decay curves (Fig. 4) exhibit a smooth decay. Nothing seems to indicate noise in their appearance. However, the chosen pulse time was clearly too short to enable complete decays.

Consequently, all data points were taken into account for the inversion and the results are shown in Fig. 5 (including resistivity, chargeability and normalized chargeability sections). The good quality of the input data is reflected by the low average model residuals, 2% for the resistivity model and 0.8% for the chargeability model.

Interpretation and discussion

Within the waste deposit area a zone of low resistivity and high chargeability stands out (Fig. 5), stretching from around 60–240 m length coordinate, which is interpreted as actual waste. The resistivity of the inverted model is less than 40 Ωm below a level that fits well with the groundwater levels documented just outside the deposit (Fig. 5a). Resistivity lies mostly in the range 100–250 Ωm in the overlying material, which can correspond to dry waste or rather coarse grained cover material and these cannot be distinguished. The whole sequence rests on highly resistive material that is most likely the bedrock, with resistivity above 1000 Ωm west of 120 m length coordinate. Resistivity below 1000 Ωm to the east may be indicative of a change in bedrock lithology.

The chargeability section (Fig. 5b) shows a strong increase in chargeability at depth varying from less than a metre to around 5 metres. This appears to correspond to the top of the waste as indicated by the maximum depth reached with the geotechnical drill rig. The normalized chargeability section appears to outline the waste body well (Fig. 5c) when plotting with a range for normalized chargeability that could be relevant for geological materials. If the range of the colour scale is stretched out a variation within the waste body becomes visible. The change in normalized chargeability at some metres depth seems to match with the groundwater level as discussed above (Fig. 5d). Below the groundwater level the variation may be due to differences in waste composition but there is no available documentation on this.

TABLE 2

Transmitted current (I), signal levels in terms of measured average potential difference for the resistance (V_R), example IP time windows ($V_{IP(1)}$ & $V_{IP(10)}$) and background potential levels (V_{backgr}) for the data recorded on the Bergaåsen test line with separated current and potential cables.

Parameter	**I/[mA]**	**V_R/[mV]**	**$V_{IP(1)}$/[mV]**	**$V_{IP(10)}$/[mV]**	**V_{backgr}/[mV]**
Range	2–50	3.7–9700	0.001–400	$3{\cdot}10^{-4}$–78	0.6–1700
Median	10	250	2.8	0.47	21

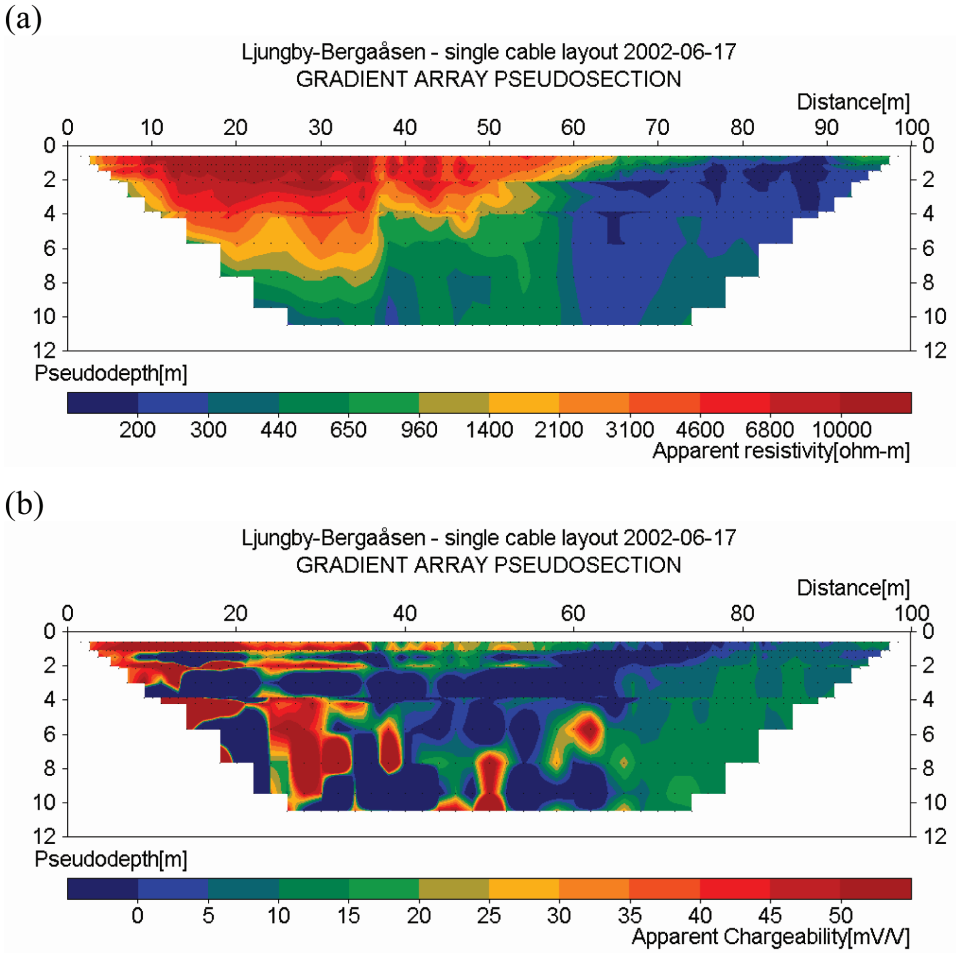

FIGURE 6

Pseudosections from the Bergaåsen site measured with single cable spread: a) resistivity, b) chargeability for time window 10–110 ms.

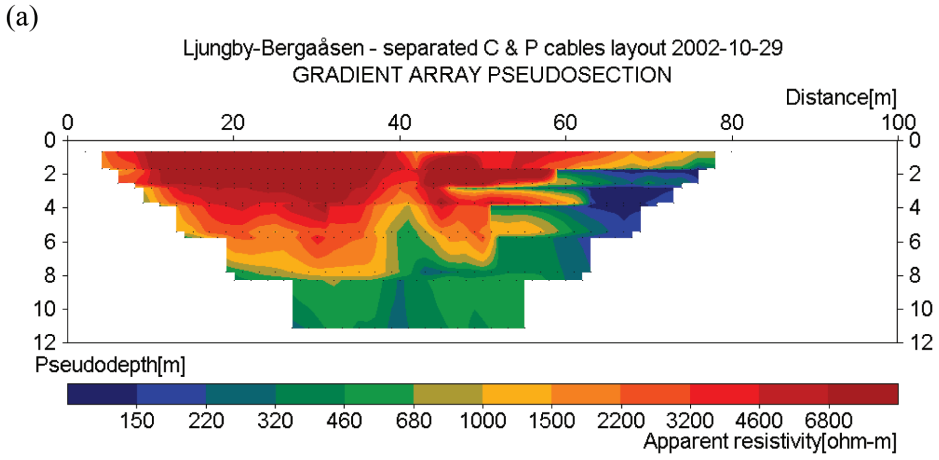

FIGURE 7
Pseudosections from the Bergaåsen test line measured with separate cable spreads for current transmission and potential measurement; a) apparent resistivity and b) apparent chargeability for time window 10–110 ms. IP decay curves from the marked areas are shown in Fig. 8.

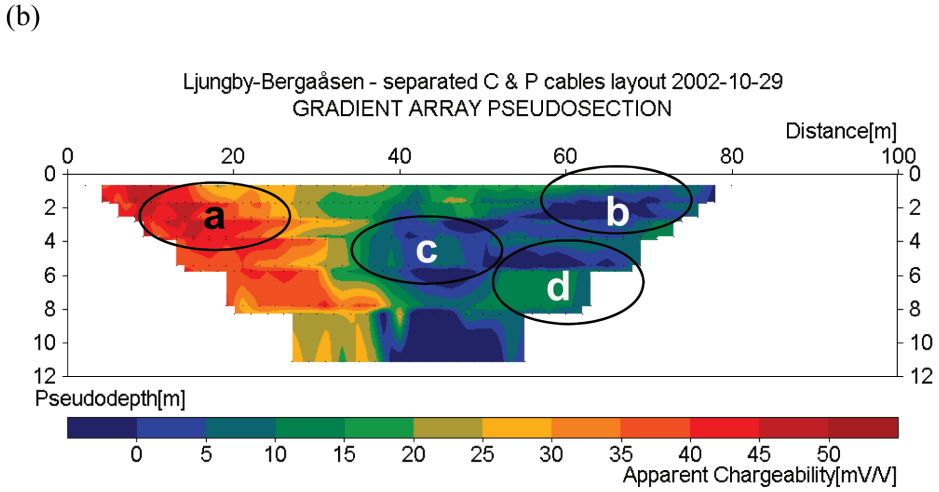

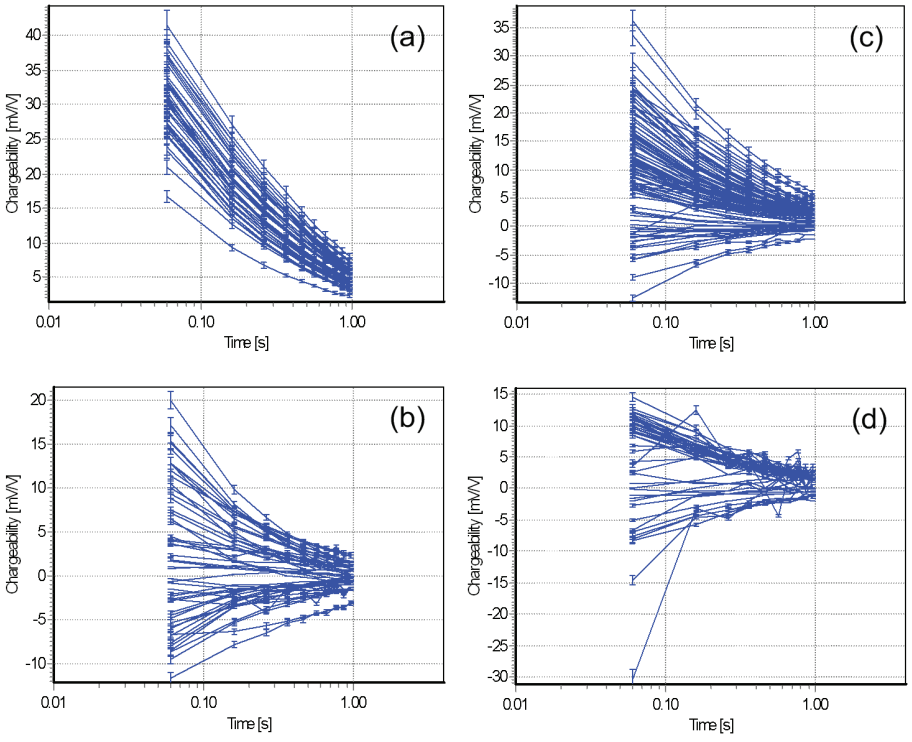

FIGURE 8
IP decay curves from the Bergaåsen test line measured with separate cable spreads for current transmission and potential measurement. The parts of the pseudosection from which each group of decay curves were gathered are marked in Fig. 7. Note that the chargeability scale differs between the diagrams.

Example 2: Bergaåsen

Site description

The Bergaåsen site, close to Ljungby in Southern Sweden is located in the glaciofluvial sediments that stretch out between the road E4 and the river Lagan. The glaciofluvial sediments constitute an aquifer that is part of the water supply of Växjö (approximately 60 000 inhabitants). At this site the increase in salt concentration due to salt applied on the road for de-icing purposes during the winter is a concern (see e.g., Leroux and Dahlin 2005). The site was included in this study on IP measurements due to the high electrode contact impedances caused by the well-drained high resistive sediments at the surface.

Data acquisition

Measurements were carried out along the test line with a single cable spread as well as with separate cable spreads. An electrode spacing of 1 m was used for both measurement sequences, employing electrode cables with 2 m take-out separation. Significant efforts were put into improving the electrode ground contact, by watering electrodes and connecting two or more electrodes to the same take-out at points with poor contact. Even so, the transmitted current was as low as 2–50 mA. The electrode contact resistances were estimated to be between a few thousand Ω and a few hundred kΩ. Two to five stacks were used for the data points, depending on the stability of the resistivity results.

Results

The signal level was in the range 4 mV to 9.7 V for the resistivity data (Table 2), with a median of 250 mV. For the IP data the signal level was a fraction of this with median values decaying from 2.8–0.47 mV from time windows 1–10 and the smallest measured signals being below the μV level. The maximum background potential level was 1700 mV.

The resistivity pseudosection measured with a single cable spread (Fig. 6a) looks smooth and consistent whereas the chargeability pseudosection (Fig. 6b) has a strongly disturbed appearance. The resistivity pseudosection measured with separated cable spreads (Fig. 7) looks quite similar to the one from the single layout, with some differences due to the difference in electrode geometry. The chargeability pseudosection has a much cleaner appearance than the one from the single spread layout and the majority of the IP decay curves now look consistent (Fig. 8). Also for this site the IP decay curves indicate that the measurement pulses were too short.

The inversion resulted in resistivity model sections with very large contrasts, where the resistivity ranges from 35 Ωm to almost 100 kΩm (Fig. 9a). Only the inversion models from the separate spread measurements are presented. The chargeability ranges from close to zero up to just above 50 mV/V (Fig. 9b), whereas the normalized chargeability is very different in appearance with maximum values reaching slightly above 0.1 mS/m (Fig. 9c). The model residuals are quite high for the resistivity (13%), probably due to the high contrasts but rather low for the IP (2.4%).

Interpretation and discussion

The inverted resistivity section shows extraordinarily high resistivity in the unsaturated glaciofluvial sand, which is a clear sign that the formation is well sorted and low in fine particles with a moisture holding capacity. This fits well with geological documentation from the site (Leroux and Dahlin 2005). The variation in resistivity in the lower layer is probably related to variation in moisture, fine material and ion content but there is no precise information available.

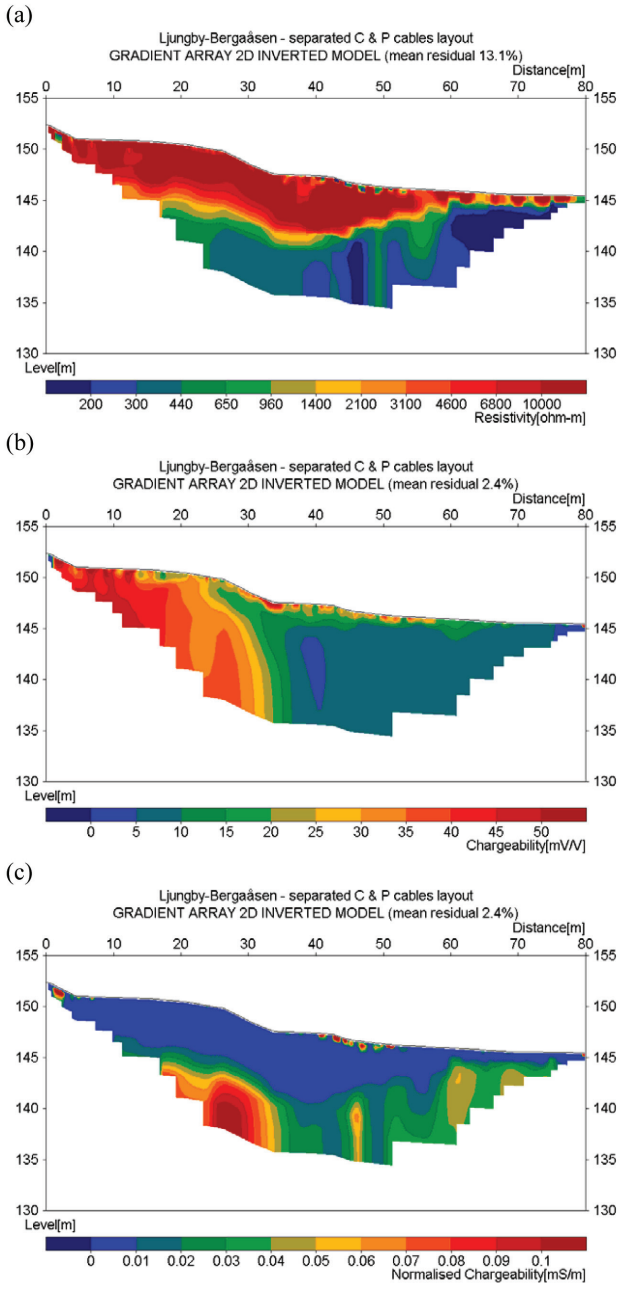

FIGURE 9

Inverted model sections based on separated cable results from Ljungby-Bergaåsen: a) resistivity, b) chargeability, c) normalized chargeability.

The chargeability exhibits a completely different pattern compared to the resistivity, with high chargeability close to the road and quite low chargeability from around 30 m length coordinate and further. One can speculate that it may be related to the salt spread on the road every winter, even if the remaining concentration is relatively low. There are also small patches with higher chargeability at the surface further on along the section.

The normalized chargeability looks to some extent as a negative image of the resistivity section. An exception is that there is a high normalized chargeability zone in the length coordinate interval 15–30 m, possibly due to a different ion content as speculated above.

Example 3: Knivsåsen – survey 1

Site description

The field tests were carried out over the Knivsåsen esker in Southern Sweden. The part of the area south of the esker is characterized by 0–20 m of till overlying aplitic gneiss, smaller areas of leptitic gneiss and dolerite intrusions. The area north of the investigated line is characterized by clayey sandy till under thin horizons of sand and/or clay. It is assumed that the till in this part of the area is underlain by sedimentary rock (Ekström 1961; Ringberg 1980). The groundwater level is very shallow in the areas surrounding the esker, as evidenced by small wetlands along the test line at the feet of the esker.

Data acquisition

Measurements were carried out using the system based on Terraohm RIP924 with both a single cable spread and with separate cable spreads for current transmission and potential measurements. As the measurements were done during different years, the location is close but not identical. An electrode separation of 5 m was used for the single cable spread measurements,

TABLE 3

Transmitted current (I), signal levels in terms of measured average potential difference for the resistance (V_R), example IP time windows ($V_{IP(1)}$ & $V_{IP(10)}$) and background potential levels (V_{backgr}) for the data recorded on the Knivsåsen test line with separated current and potential cables.

Parameter	**I/[mA]**	**V_R/[mV]**	**$V_{IP(1)}$/[mV]**	**$V_{IP(10)}$/[mV]**	**V_{backgr}/[mV]**
Range	20–200	5.3–6000	$4.4 \cdot 10^{-4}$–230	$7.5 \cdot 10^{-7}$–31	0.019–1300
Median	50	47	0.37	0.062	160

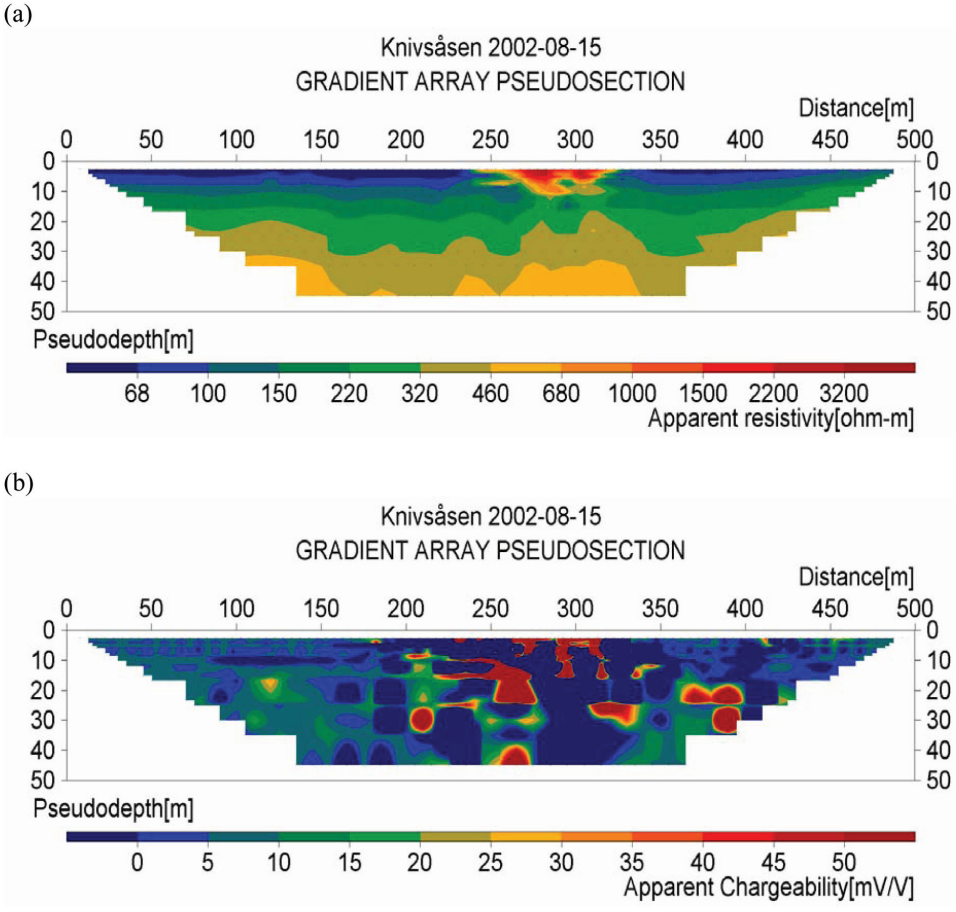

FIGURE 10

Pseudosections from the Knivsåsen site measured with single cable spread and the Terraohm RIP924 system: a) resistivity, b) chargeability for time window 10–110 ms.

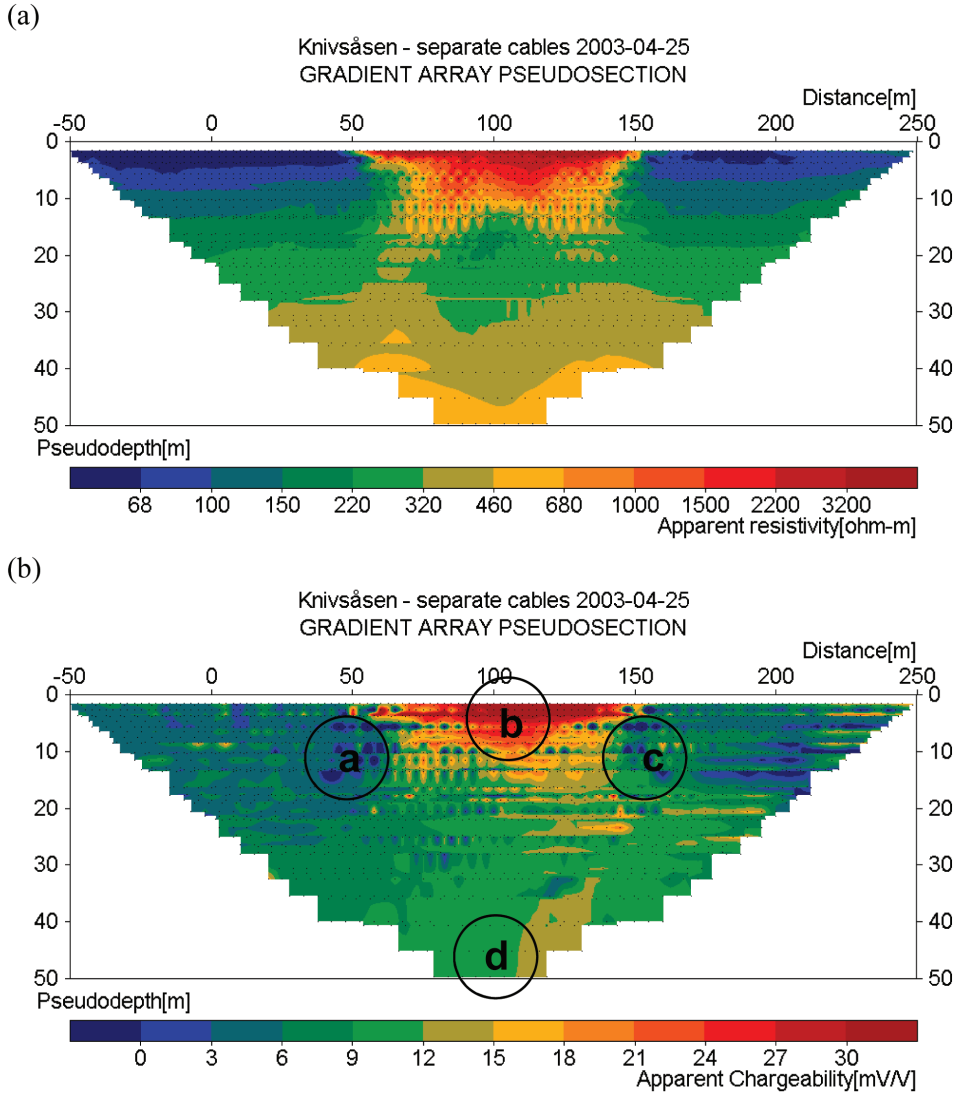

FIGURE 11
Pseudosections from the Knivsåsen test line measured with separate cable spreads for current transmission and potential measurement and the Terraohm RIP924 system; a) apparent resistivity and b) apparent chargeability for time window 10–110 ms. IP decay curves from the marked areas are shown in Fig. 12.

employing electrode cables with 5 m take-out separation. A full spread of 81 electrodes covered 400 m.

The same electrode cables were used for the separated spread layouts but the parallel cables were then shifted half an electrode take-out spacing so that the electrodes were separated by 2.5 m. Each cable spread consisted in 61 electrodes, giving a total spread cover of 300 m, which is also the total length of the line. This test line was centred over the core of the esker since that was the most interesting area in this context.

Significant efforts were put into improving the electrode ground contact in the surveys carried out both with single cable spread and separated spreads, by watering electrodes and connecting two or more electrodes to the same take-out at points with poor contact. The transmitted current was in the range 20–200 mA and the measurements were stacked two to five times. The electrode contact resistances were estimated to be in the range between a few hundred Ω to over 10 kΩ.

Results

The signal level was in the range 5 mV to 6 V for the resistivity data (Table 3), with a median of 47 mV. For the IP data the signals were a fraction of that, with median values decaying from 0.4 mV–0.06 mV from time windows 1–10 and the smallest measured signals were well below the μV level. The maximum background potential level was 1200 mV.

The resistivity pseudosection (Fig. 10a) measured with single cable spread looks very consistent, with apparent resistivities ranging from around 50 to some thousand Ωm. The chargeability pseudosection (Fig. 10b) for the first time window (10–110 ms), on the other hand, looks severely disturbed in its character, with many high- and low-apparent chargeability outliers. For the data measured with separated spreads both the resistivity and chargeability pseudosections (Fig. 11) have a consistent appearance without outliers. The slightly dotted appearance is due to the mixture of different measurement geometries in the pseudosection plots. The IP decay curves

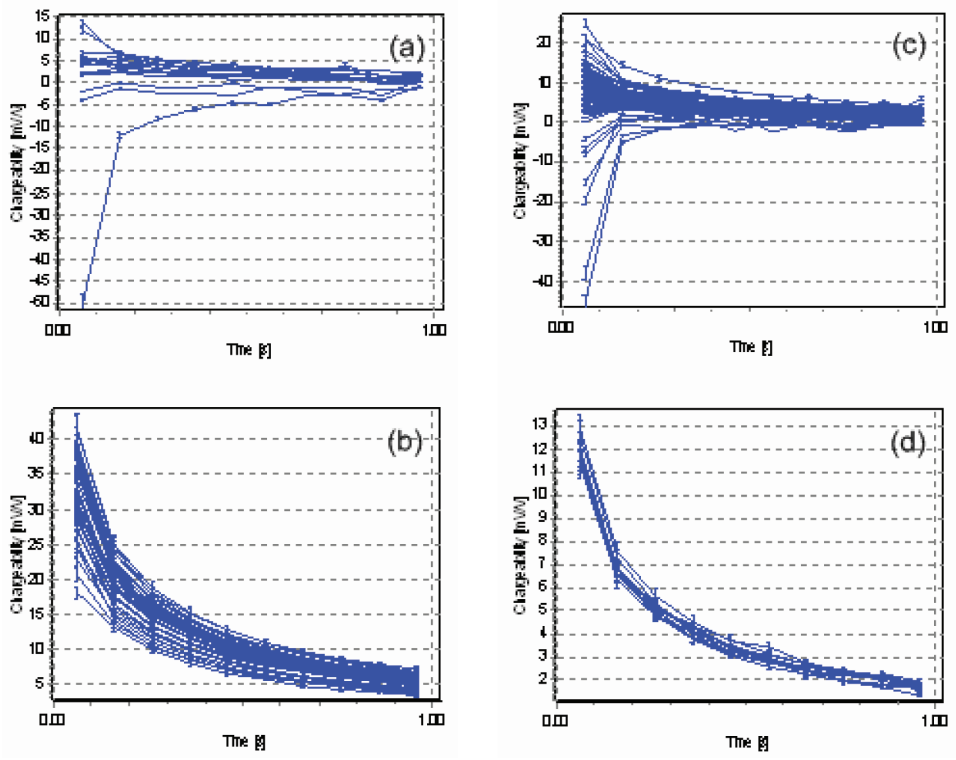

FIGURE 12
IP decay curves from the Knivsåsen test line measured with separate cable spreads for current transmission and potential measurement and the Terraohm RIP924 system. The parts of the pseudosection from which each group of decay curves were gathered are marked in Fig. 11. Note that the chargeability scale differs between the diagrams.

have smooth and continuous decays for most data points (Fig. 12), in a few cases a wavy appearance is visible at later times.

Inversion results for the data recorded with separated cable spreads are presented here and are consistent with results obtained with the single cable spread (see Dahlin and Zhou 2006). The low residuals for the inverted models emphasize the impression of good data quality, with a mean of 1.4% for the resistivity model and 2.2% for the chargeability model. As a comparison, inversion of the single spread data set gave 2.2% residual for the resistivity but 18% for the IP data. The inverted resistivity section (Fig. 13a) exhibits high contrasts with model resistivity ranging from less than 40 Ωm to more than 4000 Ωm. The inverted chargeability section (Fig. 13b) displays high chargeability in the upper part of the esker, like the resistivity. In addition there is a high chargeability zone in the deeper part of the model section in the coordinate interval 180–240 m. The normalized chargeability section (Fig. 13c) looks very different from the chargeability section, where one important difference is that the high resistivity and high chargeability zone in the upper part of the esker has low normalized chargeability. The shallow ground surrounding the esker plus the zone below the top part of the esker also display significant normalized chargeability.

For this site the IP decay curves for the highest chargeability values suggest that the measurement pulses were too short, whereas for the lower chargeability values the signals are probably below the noise level.

Interpretation and discussion

The inverted resistivity section delineates the core of the esker very distinctly, with thousands of Ωm of the dry coarse grained material protruding above the surrounding ground. Below this the groundwater level is reached and the resistivity drops to around 100 Ωm in the saturated zone. The esker is surrounded by clayey soils that are clearly outlined with resistivity values around 50 Ωm and it sits on top of high resistive bedrock.

It is noteworthy that the dry upper part of the esker has quite high chargeability but very low normalized chargeability. The soils surrounding the esker, which are dominated by clayey sandy till, have relatively high normalized chargeability, which is probably due to the mixed character of the material (see Slater and Lesmes 2002). The water saturated part of the esker exhibits moderate normalized chargeability except for the northern edge of it.

The high chargeability (moderate normalized chargeability) zone in the deeper parts of the model section in the coordinate interval 180–240 m is believed to be related to a hidden fault or dyke, with a direction consistent with regional geology. The zone is poorly covered by the separated spread data set presented here but it is visible as a low-resistive zone in the longer section measured with single cable spread as well as in parallel sections measured over the esker (Dahlin and Zhou 2006).

Example 4: Knivsåsen – survey 2

Site description

Another field test was carried out over the Knivsåsen esker. The line location was close but not identical to the test lines of the first survey.

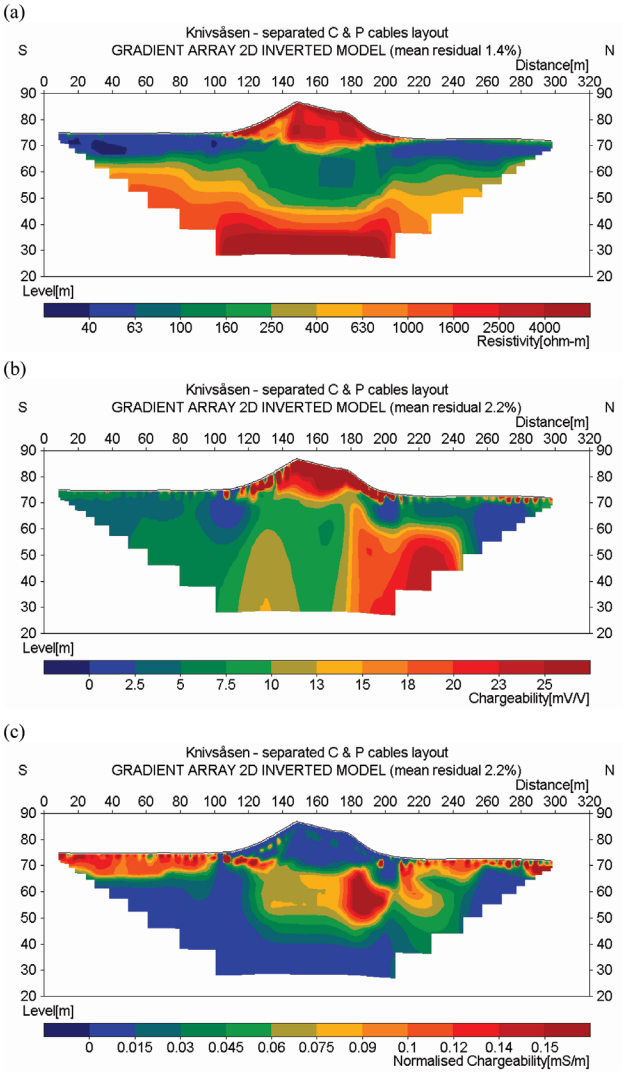

FIGURE 13

Inverted model sections based on results from separated cable and the Terraohm RIP924 system from Knivsåsen: a) resistivity, b) chargeability, c) normalized chargeability.

Data acquisition

The survey was repeated using a Terrameter LS with both single and separated cable spreads. In this case no particular efforts were made to improve the electrode ground contact. The transmitted current using this instrument was in the range 20–200 mA and 2 stacks were used for the data points. The electrode contact was measured to be in the range 480 Ω to 17 kΩ as plotted in Fig. 14.

In this survey the measurements on the separated cable spreads were taken in two steps, swapping the connection of the current and potential cable spreads in-between and using mirrored measurement protocols. This resulted in a merge of two data sets based on a mix of data where neighbouring pseudosection points are integrated over different ground volumes with similar asymmetrical but mirrored electrode geometry. For the single spread data they fall on top of each other and are averaged in the pseudosection, resulting in smoothing of the plot but for the separated spreads they end up next to each other and will thus tend to give a noisier appearance.

Results

The resistivity pseudosections (Fig. 15a and Fig. 17a) are in this case quite similar since the data point distribution differed less between the single and separated spread measurement protocols. The chargeability pseudosections for the first 20 ms time window are shown in Fig. 15b and Fig. 18b respectively. These differ significantly, with many outliers for the single cable spread. The pseudosection for the separated spread data appears noisier than the corresponding one from survey 1, as could be expected as a result of the merge of data from swapped electrode cable spreads. It should also be kept in mind that the first time window is only 20 ms long whereas in the first survey the signal is integrated over 100 ms. Furthermore, the electrode grounding was given much more attention in the first survey.

A significant number of IP decay curves look very disturbed in the single cable spread data set (Fig. 16), although a large proportion look reasonable. For the separated spread data set (Fig. 18) the majority of IP signals decay in an orderly manner.

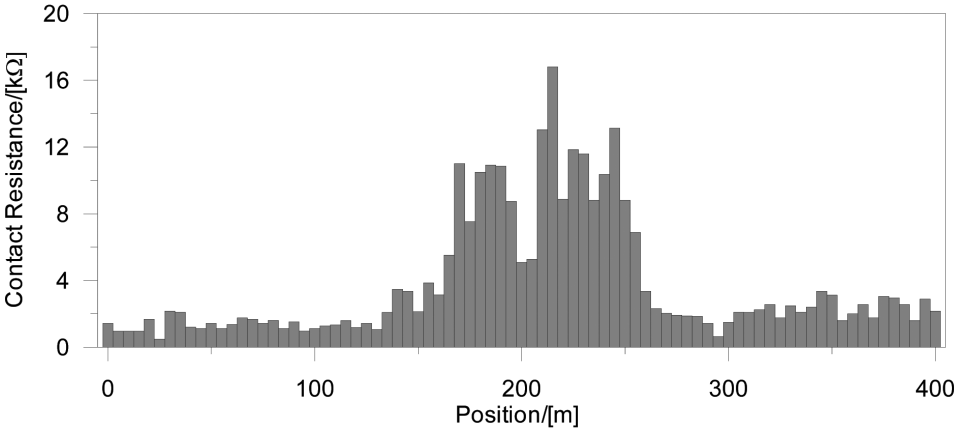

FIGURE 14

Electrode contact resistance from the Knivsåsen test line.

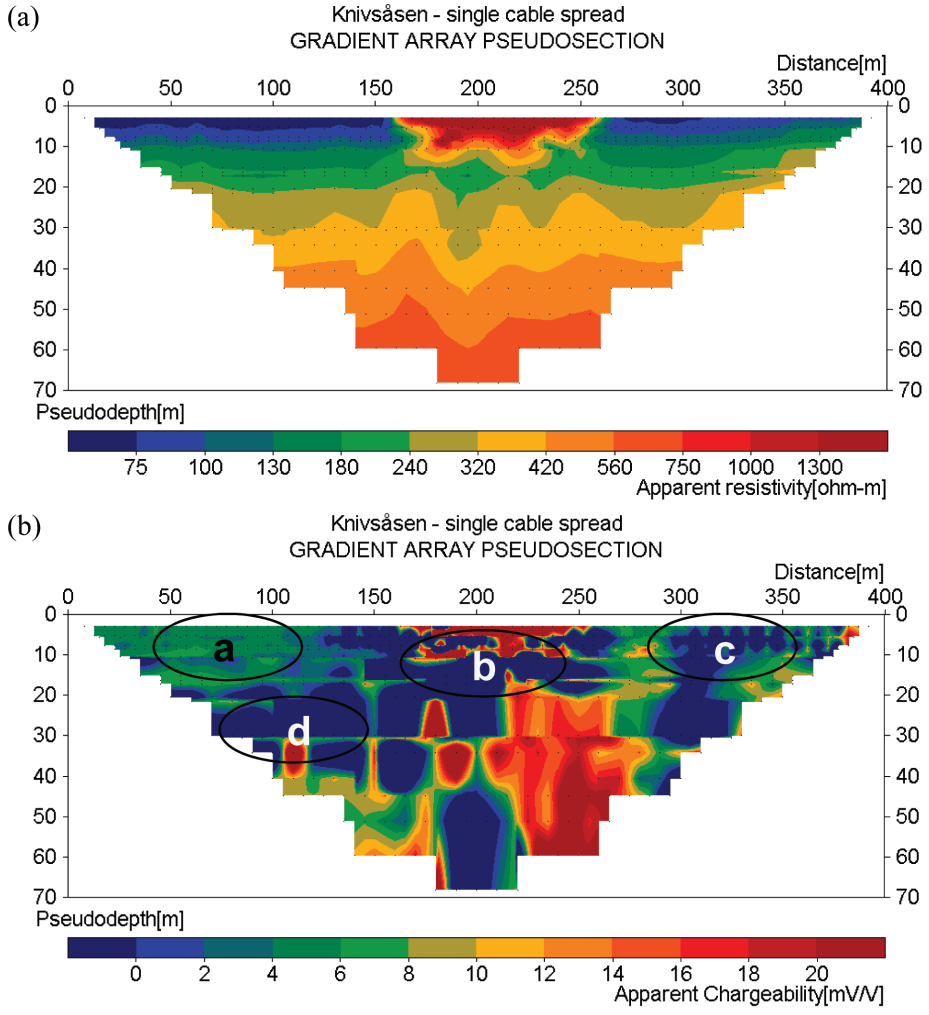

FIGURE 15
Pseudosections from the Knivsåsen test line measured with single cable spread and the ABEM Terrameter LS; a) apparent resistivity and b) apparent chargeability for time window 20–40 ms. IP decay curves from the marked areas are shown in Fig. 16.

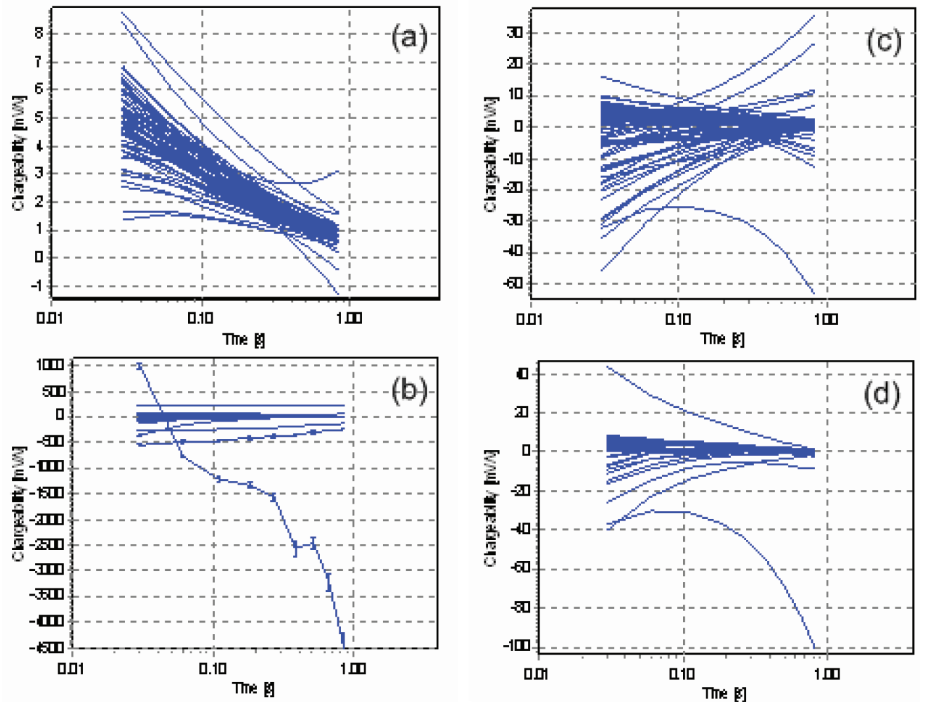

FIGURE 16
IP decay curves from the Knivsåsen test line measured with single cable spread and the ABEM Terrameter LS. The parts of the pseudosection from which each group of decay curves were gathered are marked in Fig. 15. Note that the chargeability scale differs between the diagrams.

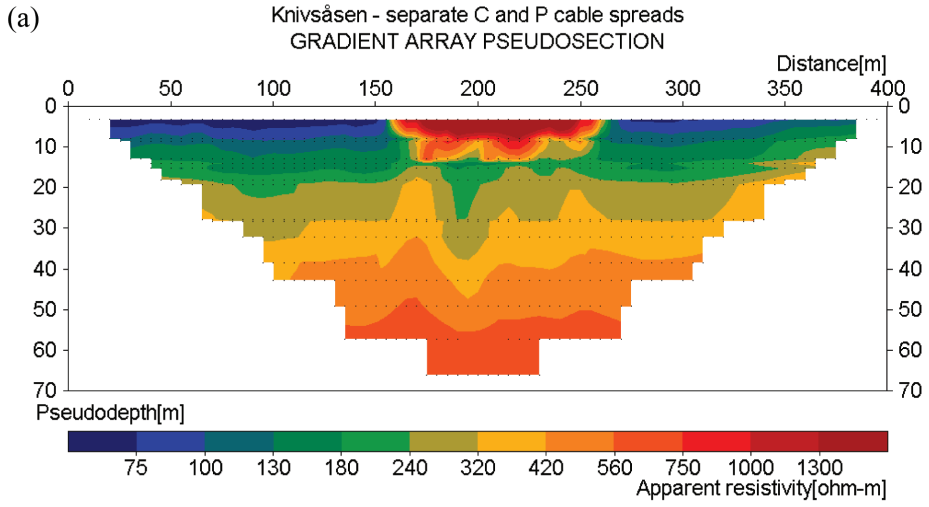

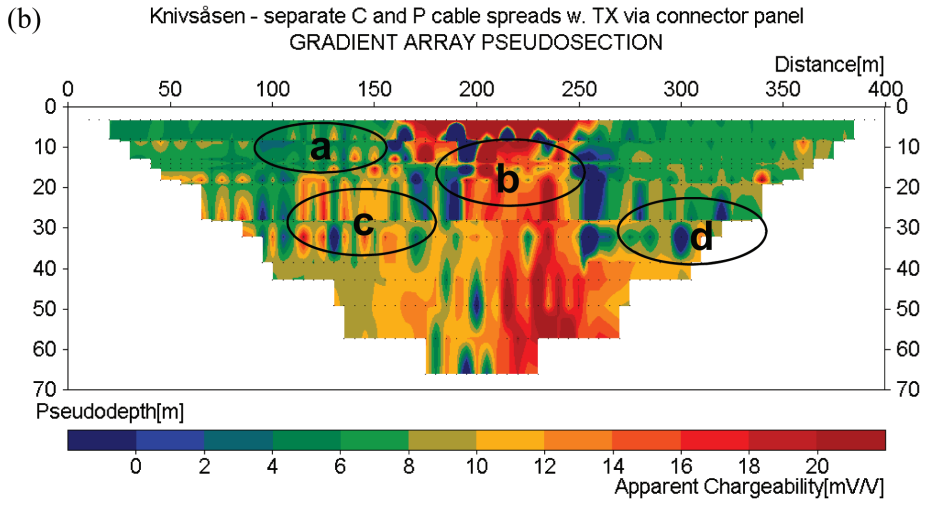

FIGURE 17
Pseudosections from the Knivsåsen test line measured with separate cable spreads for current transmission and potential measurement and the ABEM Terrameter LS; a) apparent resistivity and b) apparent chargeability for time window 20–40 ms. IP decay curves from the marked areas are shown in Fig. 18.

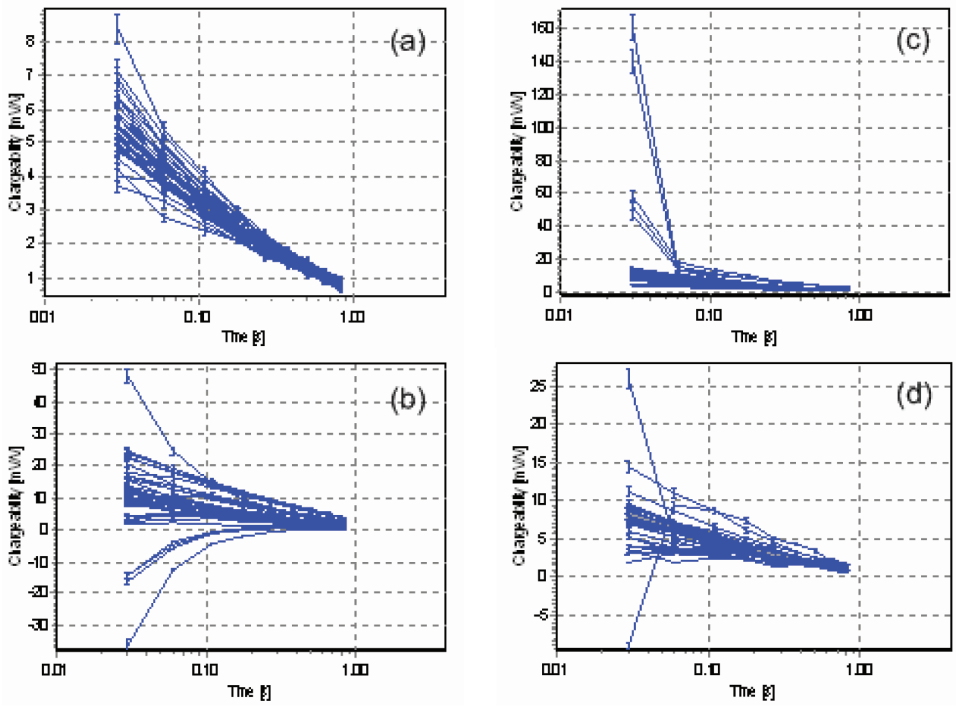

FIGURE 18
IP decay curves from the Knivsåsen test line measured with separate cable spreads for current transmission and potential measurement and the ABEM Terrameter LS. The parts of the pseudosection from which each group of decay curves were gathered are marked in Fig. 17. Note that the chargeability scale differs between the diagrams.

An example of a full waveform recording for a positive IP decay curve is shown in Fig. 19a, where power grid noise is evident. However, averaging over whole 50 Hz periods removes it efficiently. Figure 19b shows an example of a negative IP decay curve, where negative means that the measured potential immediately after the current is turned off goes beyond the rest level and then decays back towards it in the opposite direction. Negative IP effects can be explained by the relative distribution of chargeable and non-chargeable zones in the ground (e.g., Sumner 1976). Apart from power grid noise and spikes at transmitter on-off it is very consistent. An example of a data point that is affected by capacitive coupling is shown in Fig. 19c. There it is clear that the signal is strong but that the chargeability is unrealistically high.

The inversion resulted in smaller residuals than for the previous survey, 1.7% for resistivity and 4.5% for IP for the single spread data set and 1.0% for both resistivity and IP for the separated spread data set. The inverted chargeability model from the single spread data set (Fig. 20b) appears to have very poor resolution in the deeper parts. The normalized chargeability model (Fig. 20c) has an overall appearance that is similar but the chargeable zone in the lower right part is missing. Furthermore the medium chargeability of the soil layers surrounding the esker has a noisier and discontinuous appearance. The inverted model sections for the separated spread survey are quite similar to those of the previous survey difference (Fig. 21a–c) but appear to have slightly less resolution.

Interpretation and discussion

The somewhat noisier appearance in the apparent chargeability section for the core of the esker is to a large extent due to multiple electrode geometries resulting in pseudosection focus points next to each other but the lack of attention to the electrode grounding may also play a role. It is encouraging that the results agree so well in spite of this.

The results obtained with the different instrument set-ups are not directly comparable due to differences in the geometry and to less dense data coverage in the second survey. Results are however consistent in that the inverted models and the overall geological interpretation do not differ significantly between the two surveys.

The shape of the core of the esker however appears to be slightly less well resolved in the second survey using the Terrameter LS. This can simply be explained by the twice as large minimum electrode spacing used resulting in poorer data cover for the shallow parts and a coarser model grid that may result in some artefacts in an environment presenting such high contrasts in electrical properties (Dahlin and Zhou 2005). The rather large minimum electrode spacing between the potential electrodes in the separated cable spreads data set may be the reason behind the patchy appearance of the chargeability model in the core of the esker. The minimum potential electrode spacing was 10 m in the second survey and 5 m in the first. The normalized chargeability model based on the single cable spread data differs to such an extent that it would make interpretation based on it less reliable. In all cases at this site, separating current and potential cables has led to an improvement and is recommended.

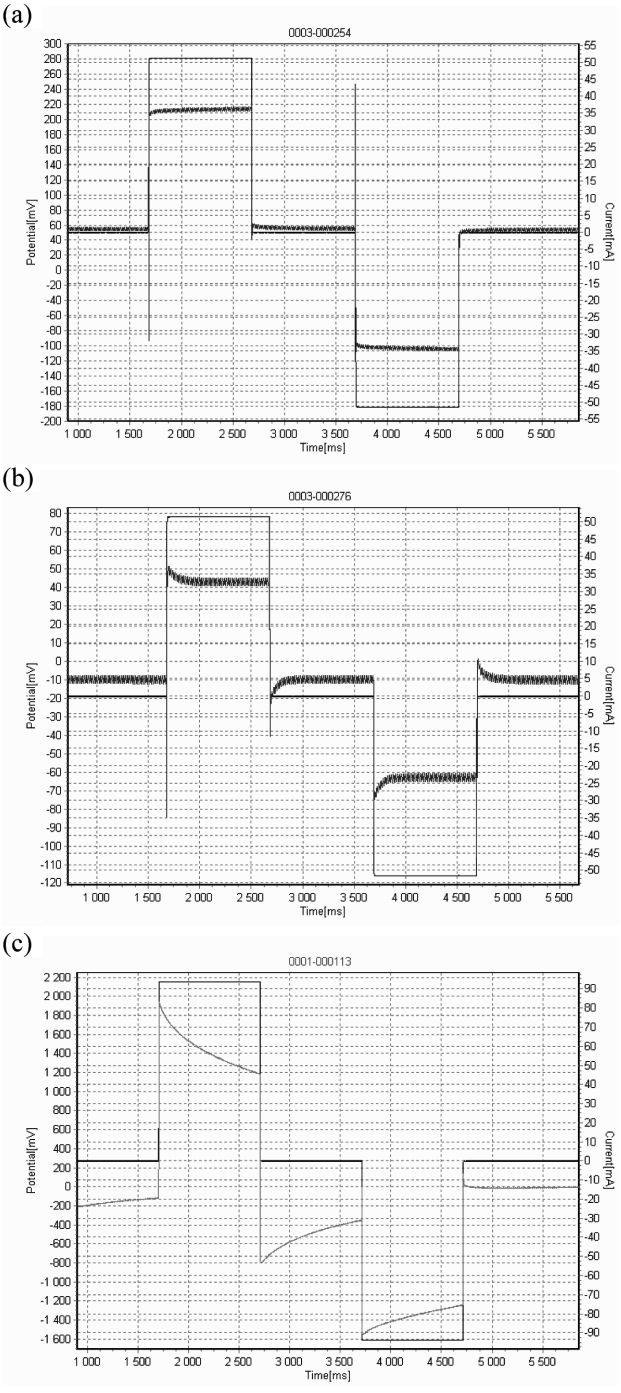

FIGURE 19

Examples of full waveform plots from the Knivsåsen site. a) Positive IP decay, b) negative IP decay, c) severe capacitive coupling.

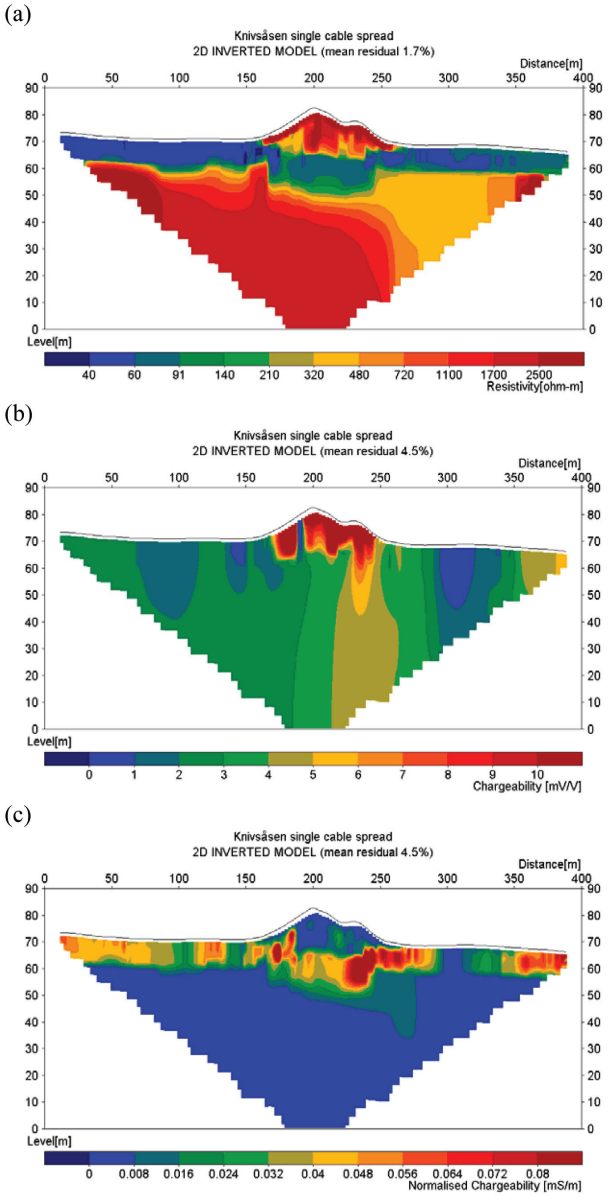

FIGURE 20
Inverted model sections based on single cable spread results with Terrameter LS from Knivsåsen: a) resistivity, b) chargeability, c) normalized chargeability.

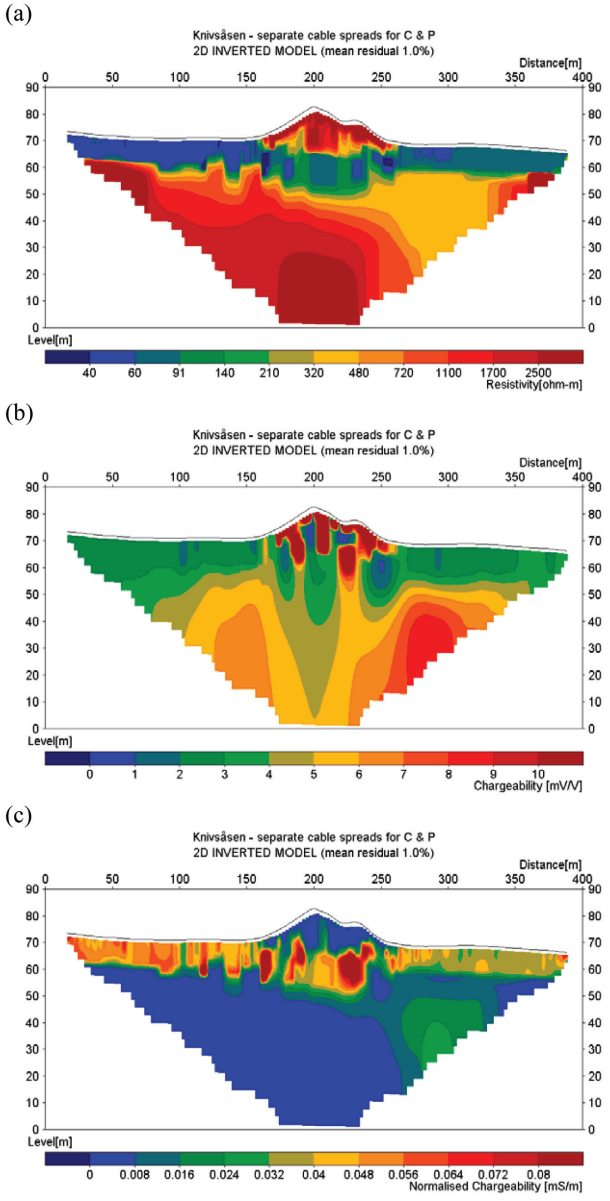

FIGURE 21
Inverted model sections based on separated cable spread results with Terrameter LS from Knivsåsen: a) resistivity, b) chargeability, c) normalized chargeability.

DISCUSSION

The results from the test sites presented here illustrate that useful induced polarization data can be obtained with multi-electrode systems. Although a precise explanation of the induced polarization phenomena observed is missing, the retrieved features are consistent with available documentation.

The first example shows that standard single spread multicore cables can be sufficient if the conditions are favourable. At this site grounding conditions are favourable and the signal levels are relatively high. These are believed to be key factors.

At the second and third sites it was necessary to separate current and potential cables to obtain consistent results. At these sites the grounding resistance was higher and signal levels were lower, as a consequence of the lower transmitted current and of smaller IP effects, particularly at the third site. The results show that separating current and potential cables can be an efficient solution for acquiring data of sufficient quality. The direct coupling between the current transmission and potential receiver conductors decreases with the square of the distance between them and this is likely to be an important factor in the improve-

ment in data quality. This arrangement also prevents the same electrodes from being used both as current and potential electrodes in the same measuring round, which may have some beneficial effects even if the electrode charge-up effects are accounted for by optimizing the measuring sequence and correcting for variation in background levels.

The procedure described for measuring with separated cable spreads is relatively simple and applicable for current field measurements but it requires an extra switching unit. For a comparable spread length a complete extra set of electrodes and cables will be required. In order to maintain the same minimum potential electrode separation and thus the same near- surface resolution twice as many electrode positions will be needed with implications for the field logistics.

The data obtained here could be interpreted using standard inverse modelling routines (Res2Dinv (Loke 2010) based on Li and Oldenburg's method (1994) and Seigel's definition of chargeability), resulting in an apparently consistent model with low residuals. The models obtained from inversion of the data agree with the general documentation at the sites, although more detailed information would be needed to fully explain the observed phenomena. It should be noted, however, that inversion that only takes the summary IP response into account only uses a fraction of the information of the IP data. Moreover, the resulting amplitude for the chargeability depends on the selected time window, since data are in general not recorded for the full decay. Methods that can make full use of the spectral information in time-domain IP data are desirable and could make time-domain data into a very powerful tool in near-surface applications. These call in their turn for more precise and 'cleaner' measurements. Realistic geological interpretation could be made even though no account was taken of possible inductive effects, other than using a 10 ms delay after current turn-off.

Assessment of data quality

Data quality assessment is always necessary before interpretation. It can be done by simple means, i.e., verifying that the pseudosections and the IP decay curves are consistent and without outliers. Full waveform should preferably be stored for more detailed data quality control and possible re-processing of the data using advanced signal processing. On the data sets measured with single cable spread at the second and third site the bad data quality could be detected directly by looking at the pseudosections, where many outliers as well as many negative chargeability data could be seen. To have a look at the decay curves can be useful in identifying noisy data; however distinguishing good and bad decay is not always so easily done.

Bertin and Loeb (1976), Sumner (1976) and Martinho and Almeida (2006), among others, have noted that measuring negative apparent induced polarization is possible under certain geometrical configurations. A negative IP decay can be due to a specific distribution of chargeable materials in the underground and/or to the electrode array used for the measurement and should not automatically be rejected. The data presented here comprise many examples of negative but consistent IP decay curves that are in good accordance with the inverted models judging by the low residuals. However, we observe that negative IP data are more common in disturbed than in good quality data, as also observed by Viezzoli *et al*. (2008). The occurrence of many negative decay curves, although possible, could be a warning sign for possible coupling effects and leads to a thorough examination of measured data. Numerical modelling on the geometrical conditions leading to negative apparent chargeability would be very useful to guide the data quality assessment.

Composite decays are theoretically possible (see Bertin and Loeb 1976) but generally it is expected that the decay should be smooth and decay in a consistent way. However it is not always the case even in what we assumed as 'good data sets' (see Figs 3, 6 and 13), even though it is more apparent in clearly noisy data (see Fig. 12).

Induced polarization decay is considered to have larger time constants than electromagnetic coupling and the difference is for instance apparent in Figs 12 and 14. However, it is not impossible that the difference in some cases is less evident and that the two effects cannot always be distinguished. This seems to advocate for including the electromagnetic effects in the calculations, although they would readily become more complex. Another strategy, would be to try to reduce these effects as much as possible.

Using the reciprocity principle to quantify the measurement quality is very useful (Parasnis 1988) and it could be used for assessing more subtle effects on IP-data, like e.g., capacitive and inductive coupling. It is, however, generally much more time consuming and thus costly, to measure the reciprocal data set than the normal data set since it is not possible to make use of the multi-channel measuring capability of the instruments to such an extent. For nested arrays, such as multiple gradient, the shorter separations between the current electrodes for reciprocal measurements will make it more difficult to transmit as much current at sites with difficult grounding conditions. Furthermore, the longer separations between the potential electrodes will tend to pick up more noise. All this will result in a decreased signal-to-noise ratio for the reciprocal data. Hence, the data quality estimations using reciprocal measurements would tend to overestimate the noise relative to the normal data set. Nevertheless checking reciprocity is useful to indicate possible problems.

Signal levels

Our results show that multi-electrode resistivity imaging type equipment can be sufficient for acquisition of IP data that can be very useful for e.g., environmental applications. Even rather modest transmitter power can be sufficient, such as the transmitter used for most of the data presented here that has a limitation of 40 W. More powerful transmitters are needed in low- resistive environments, for long layouts or for high quality demands. Transmitter output voltage is often the limiting factor for transmitting current in high-resistive environments and in the

Bergaåsen and Knivsåsen cases presented here this is the case for much of the data.

A small effective input signal is often a limiting factor, as illustrated by the examples presented here. The signal levels are magnitudes lower for IP measurements than for resistivity measurements, especially in natural soils where the IP effects are usually relatively small. The signal levels are often much higher in waste but still a factor of ten, or more, smaller than for the resistivity measurements. In addition, the IP signals are generally integrated over much shorter time intervals than the resistivity signals and this means that the effective resolution of the AD-converter is smaller.

The small effective signals mean that it is important to select an electrode array with good signal strength, i.e., electrode arrays with a large geometrical factor should be avoided. This generally makes dipole-dipole array a poor choice from a signal-to-noise point of view, whereas a multiple gradient array that was used here is more favourable (e.g., Dahlin and Zhou 2006). As pointed out earlier, the dipole-dipole array has traditionally been used extensively for IP surveying in order to minimize coupling problems but it does not offer any advantage when measuring with the type of multi-electrode equipment used here.

The electrode contact is a key factor, as good contact allows more current to be transmitted, whereas the signal will easier drown in noise if less current is transmitted. Furthermore high contact resistance will enhance capacitive coupling. Stainless steel electrodes were used in all the examples presented here. A major advantage of steel electrodes is that they are easy to handle and can take a lot of rough treatment, which makes it easier to provide good ground contact (lower contact resistance). A drawback of stainless steel electrodes is the background potentials due to electrochemical processes between the electrode and the ground being large compared to non-polarizable electrodes (Dahlin *et al*. 2002). Furthermore, the electrodes are charged when used for transmitting current and it can take several tens of minutes before these potentials have decayed (Dahlin 2000).

The signals arising from the transmitted current are superimposed on background potentials that exist between the receiving electrodes and they can vary significantly during the measurement. In all the examples presented here the background potentials are hundreds of mV for many of the data points and a significant number of them reach well above 1 V. This means that it is essential to have an instrument with high-dynamic resolution in order to resolve the small induced signals on top of the background potentials, whereas a high amplification rate would be of limited use. Since the best resolution input range of the instrument used in the last example is ±2.5 V it can be expected to use the best resolution regardless of electrode polarization, which is important for small induced potentials. The theoretical resolution is 3 nV at 1 s integration for this measurement range but the actual resolution is lower for shorter integration times and with ambient noise present. If the best resolution input range was for example ±250 mV it could not be used for a large amount of the measurements at the test lines presented here even if the induced signals were small. This could become problematic if the input section of the instrument was based on an AD-converter with less resolution. It should be noted that it is essential to correct for the varying background levels, otherwise large errors will occur in both the resistivity and IP data.

Timing considerations

A further complication is that the short time between current turn-off and start of signal integration makes IP measurement much more prone to signal disturbances from coupling. Coupling can arise for example between different cables, between the conductors inside the electrode cables, between different conductors inside the instrument and between cables and the ground. Our results suggest that coupling inside the electrode cables dominates for the latter two sites and that much of the noise due to coupling can be removed by separating the cable spreads used for current transmission and potential measurement. It would however be useful to look further into the other coupling mechanisms, in order to identify measuring situations in which they would be significant and if possible develop tools for automatic data quality assessment.

The fact that the pulse length was generally too short leads to underestimation of the DC resistivity values since the current-on voltage signals have not reached their full values. The IP effects will also be affected, where the exact impact is complex due to repeated current pulses with different polarity that counteract each other. This also has consequences for the correction applied for the background potential. The pulse length chosen will often in actual surveys tend to be too short in relation to the decay times since it immediately affects the time spent on field data acquisition and using a longer pulse time will make the field survey more time consuming and thus more expensive.

CONCLUSIONS

Useful and apparently reliable data were obtained with the procedures described here. It is possible to obtain good quality IP data using multi-electrode resistivity-IP equipment and single spread electrode cable layouts at sites with favourable electrode contact, sufficient signal levels and low noise levels, as illustrated by the Ekeboda example.

Sites with high contact resistances often result in low signal levels and noise problems, which are most likely due to capacitive coupling, making the IP signals drown in noise, as illustrated by the Bergaåsen and Knivsåsen examples. In such cases it can be possible to obtain useful and interpretable time-domain IP data with conventional multi-electrode resistivity-IP equipment by using separate cable spreads for transmitting current and measuring potentials. The procedure described for measuring with separated cable spreads is relatively simple and applicable for current field measurements.

The resulting models agree with the general documentation at the sites, although more detailed information would be needed to

fully explain the observed phenomena. Comparison with relevant field documentation and well-designed laboratory experiments are necessary for a better understanding.

Data quality assessment is always necessary before interpretation. It can be done by simple means, i.e., verifying that the pseudosections and the IP decay curves are consistent and without outliers.

Using the reciprocity principle would presumably be useful when assessing more subtle effects on IP-data, like e.g., capacitive and inductive coupling but it would be much more than twice as time consuming and would tend to overestimate the noise for nested electrode arrays. It is the reason why it is seldom completely undertaken.

IP responses can be negative due to the relative positions of chargeable and non-chargeable zones, as exemplified here but negative IP data may also arise from noise due to coupling. It would be useful to more precisely define when such curves can be expected.

The data obtained here could be interpreted using standard inverse modelling routines and using summarized chargeability for all time windows, resulting in models that add significant information to the resistivity models. Methods that can make full use of the spectral information in time-domain IP data are desirable as potentially a significant amount of useful information is not being made available to the interpreter.

ACKNOWLEDGEMENTS

We acknowledge the help of several people, students at the time, in gathering field data: Anna-Karin Jönsson, Alfredo Mendoza, Ola Mårtensson, Pontus Pojmark and Benedict Rumpf. The measurements on the Ekeboda landfill were made by Björn Johansson and Sonja Jones.

We wish to thank the associate editor Andreas Hördt, plus Andreas Weller and an anonymous reviewer, for constructive criticism that helped us improve the quality of this manuscript.

REFERENCES

Abu-Zeid N., Bianchini G., Santarato G. and Vaccaro C. 2003. Geochemical characterization and geophysical mapping of landfill leachates: The Marozzocanal case study (NE Italy). *Environmental Geology* **45**, 439–447.

Bertin J. and Loeb J. 1976. *Experimental and Theoretical Aspects of Induced Polarization, Vol I and II*. Gebrüder Borntraeger, Berlin-Stuttgart, 335p.

Carlson N.R., Mayerle C.M. and Zonge K.L. 1999. Extremely fast IP used to delineate buried landfills. *Proceedings of the 5th meeting of the EEGS, European Section,* Budapest, Hungary, Ch3.

Collett L.S. 1990. History of the induced polarisation method. In: *Induced polarization: Applications and case histories*, (eds. J.B. Fink, E.O. McAlister, B.K. Sternberg, S.H. Ward and W.G. Wieduwilt), pp. 5–22. Society of Exploration Geophysicists, Invest. Geophys. 4.

Dahlin T. 2000. Electrode charge-up effects in DC resistivity data acquisition using multi electrode arrays. *Geophysical Prospecting* **48**(1), 181–187.

Dahlin T., Leroux V. and Nissen J. 2002. Measuring techniques in induced polarisation imaging. *Journal of Applied Geophysics* **50**(3), 279–298.

Dahlin T., Rosqvist H. and Leroux V. 2010. Resistivity-IP mapping for landfill applications. *First Break* **28**, 101–105.

Dahlin T. and Zhou B. 2006. Gradient array measurements for multi-channel 2D resistivity imaging. *Near Surface Geophysics* **4**, 113–123.

Ekström G. 1961. *Beskrivning till kartbladet Revinge*. Serie Ad, Nr 3, Sveriges Geologiska Undersökning (Swedish Geological Survey), Stockholm, 66p.

Ghorbani A., Camerlynck C., Florsch N., Cosenza P. and Revil A. 2007. Bayesian inference of the Cole–Cole parameters from time- and frequency-domain induced polarization. *Geophysical Prospecting* **55**, 589–605.

Hohmann G.W. 1973. Electromagnetic coupling between grounded wires at the surface of a two-layered earth. *Geophysics* **38**(3), 854–863.

Hördt A., Blaschek R., Kemna A. and Zisser A. 2007. Hydraulic conductivity estimation from induced polarisation data at the field scale – The Krauthausen case history. *Journal of Applied Geophysics* **62**, 33–46.

Hördt A., Hanstein T., Hönig M. and Neubauer F.M. 2006. Efficient spectral IP-modelling in the time domain. *Journal of Applied Geophysics* **59**, 152–161.

Iliceto V. and Morelli G. 1999. Environmental assessment of municipal waste dump sites with electrical resistivity and induced polarization multielectrode methods. In: *Proceedings of the 5th meeting of the EEGS (Environmental and Engineering Geophysics Society) – European Section,* Budapest, Hungary, September 6–9, Ch 4.

Johansson B. and Jones S. 2007. *Ekebodadeponin I Hörby: Utbredning, lakvattenspridning och påverkan på omgivning – En geofysisk undersökning med mätningar av resistivitet och inducerad polarisation* (in Swedish), M.Sc. thesis, Engineering Geology, Lund University, ISRN LUTVDG/TVTG--5103—SE, 71p.

Johansson B., Jones S., Dahlin T. and Flyhammar P. 2007. Comparisons of 2D and 3D inverted resistivity data as well as resistivity and IP surveys on a landfill. *Proceedings of the 13th Near Surface Geophysics Conference, EAGE,* Istanbul, Turkey, 3–5 September, P42.

LaBrecque D. and Daily W. 2008. Assessment of measurement errors for galvanic-resistivity electrodes of different composition. *Geophysics* **73**(2), F55–F64.

Leroux V. and Dahlin T. 2005. Time-lapse resistivity investigations for imaging saltwater infiltration in glaciofluvial deposits. *Environmental Geology* **49**(3), 347–358.

Loke M.H. 2011. *Tutorial: 2-D and 3-D electrical imaging surveys*. Available at www.geoelectrical.com

Major J. and Silic J. 1981. Restrictions on the use of Cole-Cole dispersion models in complex resistivity interpretation. *Geophysics* **41**, 916–931.

Martinho E. and Almeida F. 2006. 3D behavior of contamination in landfill sites using 2D resistivity/IP imaging: Cases studies in Portugal. *Environmental Geology* **49**, 1071–1078.

Nielsen T.I. 2006. The effect of electrode contact resistance and capacitive coupling on complex resistivity measurements (2006). *SEG Expanded Abstracts* **25**(1), 1376–1380.

Nielsen T.I. and Baumgartner F. 2006. Numerical modeling of complex resistivity effects on a homogeneous half-space at low frequencies. *Geophysical Prospecting* **54**, 261–271.

Oldenburg D.W and Li Y. 1994. Inversion of induced polarization data. *Geophysics* **59**, 1327–1341.

Parasnis D.S. 1988. Tutorial: Reciprocity theorems in geoelectric and geoelectromagnetic work. *Geoexploration* **25**, 177–198.

Pelton S.H., Ward S.H., Hallof P.G., Sill W.R. and Nelson P.H. 1978. Mineral discrimination and removal of inductive coupling with multi-frequency IP. *Geophysics* **43**, 588–609.

Radic T. 2004. Elimination of cable effects while multi-channel SIP measurements. *Proceedings of the 10th EEGS-ES meeting*, Utrecht, the Netherlands, P029.

Ringberg B. 1980. *Beskrivning till jordartskartan Malmö SO* (in Swedish), Serie AE, Nr 38, Sveriges Geologiska Undersökning (Swedish Geological Survey), Uppsala, 179p.

Routh P.S. and Oldenburg D.W. 2001. Electromagnetic coupling in frequency-domain induced polarization data: A method for removal. *Geophysical Journal International* **145**, 59–76.

Seigel H., Nabighian M., Parasnis D.S. and Vozoff K. 2007. The early history of the induced polarization method. *The Leading Edge* **3**, 312–321.

SGU. 2000. *Förslag till skyddsområden för Hörby kommuns samtliga vattentäkter* (in Swedish), Uppsala.

Slater L. and Lesmes D. 2002. IP interpretation in environmental investigations. *Geophysics* **67**, 7788.

Sogade J.A., Scira-Scappuzzo F., Vichabian Y., Shi W., Rodi W., Lesmes D.P. and Morgan F.D. 2006. Induced-polarization detection and mapping of contaminant plumes. *Geophysics* **71**(3), B75–B84.

Soininen H. 1984. Inapplicability of pulse-train time-domain measurements to spectral induced polarization. *Geophysics* **49**(6), 826–827.

Sumner J.S. 1976. *Principles of Induced Polarization for Geophysical Exploration*. Developments in Economic Geology 5, Elsevier, Amsterdam, 277p.

Swift C.M. and Hohmann G.W. 1975. Discussion on "EM coupling, its intrinsic value, its removal and the cultural coupling problem" by J.C. Wynn and K.L. Zonge (1975). *Geophysics* **41**, 543.

Vacquier V. 1957. Prospecting for ground water by induced electrical polarization. *Geophysics* **22**(3), 660–687.

Viezzoli A., Pedersen J. and Pytlich A. 2008. Quantitative appraisal of noise in time-domain induced polarization data. *Proceedings of Near-Surface 2008, 14th European Meeting of Environmental and Engineering Geophysics,* Kraków, Poland, 15–17 September. EAGE eds, A32.

Wait J.R. and Gruszka T.P. 1986. On electromagnetic coupling removal from induced polarization surveys. *Geoexploration* **24**, 21–27.

Zonge K. L., Sauck W. A. and Sumner J.S. 1972. Comparison of Time, Frequency, and Phase Measurements in Induced Polarization. *Geophysical Prospecting* **20**, 626–648.